Journal of Alloys and Compounds, *176* (1991) 215–224
LCM 1114

Phase relations of the Sm–Fe–Ti system around the compound $SmFe_{11}Ti$

Yoon-Bae Kim*, Satoshi Sugimoto, Masuo Okada and Motofumi Homma
Department of Materials Science, Faculty of Engineering, Tohoku University, Sendai 980 (Japan)

(Received September 24, 1990; in final form December 17, 1990)

Abstract

Phase relations of the Sm–Fe–Ti system were studied, especially surrounding the compound $SmFe_{11}Ti$. Isothermal sections of the iron-rich corner of the Sm–Fe–Ti system were constructed, based tentatively on microstructural studies. The as cast $SmFe_{11}Ti$ alloy was nearly single phase with a $ThMn_{12}$-type structure. It was found that the phases α-Fe(Ti), Fe_2Ti, $Fe_{17}Sm_2$, Fe_3Sm and Fe_2Sm exist around the composition of the $SmFe_{11}Ti$ compound after annealing at 800 °C. After annealing at 1000 °C, a liquid and a high temperature phase exist instead of the Fe_3Sm and Fe_2Sm phases. The high temperature phase, which is believed to be non-magnetic or weakly magnetic, was observed in samarium-rich alloys with high titanium content. The composition of this high temperature phase was identified as $SmFe_9Ti_2$ by scanning electron microscopy and energy-dispersive X-rays. In the melt-spun samples, the $SmFe_{11}Ti$ showed the highest coercivity of the alloys studied. The course of coercivity of melt-spun samples revealed that coercivity is most sensitive to samarium content among the components of the Sm–Fe–Ti system.

1. Introduction

Recent work on the magnetic properties of RE(Fe, M)$_{12}$-type compounds with $ThMn_{12}$ structure have shown that the RE(Fe, M)$_{12}$ compound is a possible new candidate for permanent magnets [1, 2]. Among the reported RE(Fe, M)$_{12}$ compounds, RE ≡ Sm seems to be the most suitable candidate for permanent magnetic materials because of its sufficient magnetocrystalline anisotropy with relatively high magnetization and high Curie temperature [1–3]. Much effort, therefore, has been focused on the samarium-containing $ThMn_{12}$-type compounds to obtain high coercivity. For example, high coercivities have been observed in melt-spun Sm–Fe–Ti samples [4]. High coercivities of 6.5 kOe and 7.7 kOe were reported in Sm–Fe–Ti–B and Sm–Fe–Ti–(Al, Si) melt-spun ribbons [5]. The highest coercivities in $ThMn_{12}$-type compounds were recorded for $SmFe_{10}$(Ti, V) by melt-spinning (12 kOe) [6] and for the Sm–Fe–V system as by mechanical alloying (11.7 kOe) [7].

*Present address: The Magnetic Laboratory, Korea Standards Research Institute, P.O. Box 3, Taedok Science Town, Taejon, Ch'ungnam 302–340 (Korea).

0925-8388/91/$3.50

Recently, the magnetic properties of ternary Sm(Fe, M)$_{12}$ compounds, (M ≡ Ti, Si, V, Cr and Mo) were studied by Ohashi *et al.* [8]. In that investigation the $SmFe_{11}Ti$ compound (M ≡ Ti) showed the highest values in saturation magnetization, Curie temperature and anisotropy field among the alloys studied. This result suggests that the ternary Sm–Fe–Ti system is the most promising candidate for producing $ThMn_{12}$-type permanent magnets.

A basic understanding of the phase relations in the Sm–Fe–Ti system is urgently required. Jang and Stadelmaier [9] reported the isothermal phase diagram of Sm–Fe–Ti at 900 °C, but the optimum annealing temperature for Sm–Fe–Ti melt-spun ribbons giving the high coercivity, lies in the range 750–850 °C [5, 6]. Because of practical interest in Sm–Fe–Ti alloys as candidates for permanent magnets, establishment of the phase relations at 800 °C around the compound $SmFe_{11}Ti$ are strongly required. Since the evaporation of samarium from the sample during annealing is very severe, a short-annealing time was adopted in the present study for constructing accurate phase relations. This means that the present study aims to construct the tentative non-equilibrium isothermal sections of the iron-rich corner of the Sm–Fe–Ti system. The relationship between the phase-relations and magnetic properties of Sm–Fe–Ti alloys is discussed.

2. Experimental procedures

Sixteen alloys with compositions $Sm_xFe_{100-x-y}Ti_y$ ($3.8<x<11.5$, $3.8<y<19.2$) surrounding the $SmFe_{11}Ti$ (12–1) compound were prepared by induction melting in an argon atmosphere. The compositions and sample numbers of the ingots and the preparation procedures are presented in Fig. 1. The alloys $Sm_{7.7}Fe_{88.5}Ti_{7.7}$ (sample 8) and $Sm_{7.7}Fe_{76.9}Ti_{15.4}$ (sample 10) correspond to $SmFe_{11}Ti$ and $SmFe_{10}Ti_2$ respectively. To investigate the phase relationship around $SmFe_{11}Ti$, the microstructures of as-cast samples and samples annealed at 800–1000 °C for 4 h in argon were investigated by X-ray diffraction using Fe Kα radiation, optical microscopy and scanning electron microscopy with energy-dispersive X-rays (SEM–EDX). Magnetic properties of annealed samples were also measured and the correlation with microstructure was investigated. Annealing temperatures for cast ingots were chosen to be 800 °C and 1000 °C because the former temperature is very close to the optimum annealing temperature for overquenched Sm(Fe, Ti)$_{12}$ or Sm(Fe, Ti, M)$_{12}$ melt-spun ribbons, and the latter temperature is near the homogenization temperature for cast ingots [4–8].

Overquenched melt-spun ribbons of $Sm_xFe_{100-x-y}Ti_y$ alloys were prepared by applying a surface velocity of 40 ms^{-1} using a single copper wheel in argon. The fabricated flake ribbons were about 20 μm × 1 mm × 50 mm in size. The ribbons were annealed at 800 °C for 30 min in a samarium atmosphere [6, 10].

To measure the magnetic properties, ingot or ribbon samples were ground into powders under 200 μm in size by hand milling. Then, the powders were

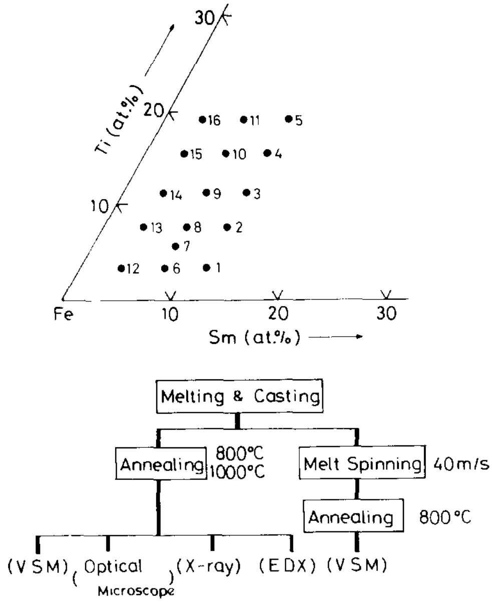

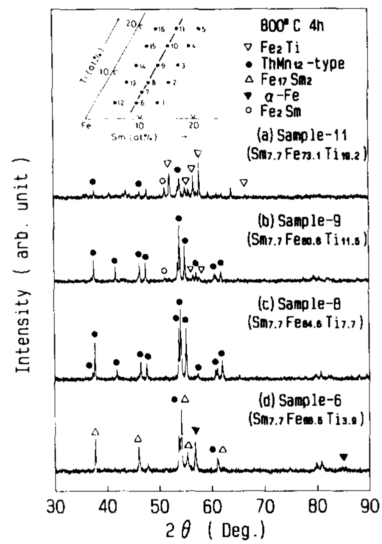

Fig. 1. The compositions, sample numbers and the preparation of the alloys in the Sm–Fe–Ti system.

Fig. 2. X-ray diffraction patterns of (a) $Sm_{7.7}Fe_{73.1}Ti_{19.2}$ (sample 11), (b) $Sm_{7.7}Fe_{80.8}Ti_{11.5}$ (sample 9), (c) $Sm_{7.7}Fe_{84.6}Ti_{7.7}$ (sample 8), and (d) $Sm_{7.7}Fe_{88.5}Ti_{3.9}$ (sample 6) annealed at 800 °C for 4 h.

aligned in a magnetic field of 12 kOe (0.96 MA m^{-1}) in molten paraffin and solidified. The magnetic properties were measured by a vibrating sample magnetometer (VSM) with a maximum applied field of 15 kOe (1.2 MA m^{-1}).

3. Results and discussion

3.1. Isothermal section of the Sm–Fe–Ti system for the iron-rich corner at 800 °C

Figure 2 shows typical X-ray diffraction patterns obtained from $Sm_{7.7}Fe_{72.3-y}Ti_y$ ($3.8<y<19.2$) alloys annealed at 800 °C for 4 h. The diffraction peaks of the Fe_2Ti and Fe_2Sm phases can be observed in titanium-rich alloys such as $Sm_{7.7}Fe_{73.1}Ti_{19.2}$ (sample 11) and $Sm_{7.7}Fe_{80.8}Ti_{11.5}$ (sample 9) (Figs. 2(a) and (b)). It can be seen that the intensity of the Fe_2Ti diffraction peaks becomes stronger as the titanium content increases. Figure 2(c) shows that the $Sm_{7.7}Fe_{84.6}Ti_{7.7}$ (sample 8) composition corresponds to the $SmFe_{11}Ti$ (12–1) compound, and is nearly single phase with the tetragonal $ThMn_{12}$ structure, as reported in refs. 2 and 11. The titanium-poor alloy $Sm_{7.7}Fe_{80.5}Ti_{3.9}$ (sample 6) contains the α-Fe(Ti) phase (see Fig. 2(d)). However, using only X-ray diffraction, it is difficult to clarify whether the $Fe_{17}Sm_2$ phase exists or not, because the diffraction peaks of the $ThMn_{12}$-type phase and $Fe_{17}Sm_2$ (17–2) almost overlap each other.

Figure 3 shows the microstructures of (a) $Sm_{7.7}Fe_{73.1}Ti_{19.2}$ (sample 11), (b) $Sm_{7.7}Fe_{80.8}Ti_{11.5}$ (sample 9), and (c) $Sm_{7.7}Fe_{88.5}Ti_{3.9}$ (sample 6) annealed at 800 °C for 4 h and then quenched in water. The $Sm_{7.7}Fe_{73.1}Ti_{19.2}$ (sample 11) and $Sm_{7.7}Fe_{80.8}Ti_{11.5}$ (sample 9) are composed of four phases: Fe_2Ti, $SmFe_{11}Ti$ (12–1), and a mixture of $Fe_{17}Sm_2$ and a titanium-rich phase (Figs. 3(a) and (b)). It can be said that these alloys are inhomogeneous after annealing at 800 °C for 4 h and that the annealing time is too short to homogenize these alloys. In the $Sm_{7.7}Fe_{88.5}Ti_{3.9}$ alloy (sample 6), only the two phases $Fe_{17}Sm_2$ and α-Fe(Ti) can be observed (Fig. 3(c)).

Figure 4 shows the X-ray diffraction patterns taken from $Sm_xFe_{92.3-x}Ti_{7.7}$ $(3.8<x<11.5)$ alloys annealed at 800 °C for 4 h. It is found that the $Sm_{3.8}Fe_{88.5}Ti_{7.7}$ alloy (sample 13) contains the α-Fe(Ti) phase in addition to the $SmFe_{11}Ti$ (12–1) and Fe_2Ti phases. The $Sm_{7.7}Fe_{84.6}Ti_{7.7}$ alloy (sample 8) is nearly single phase with $ThMn_{12}$-type structure. In the $Sm_{11.5}Fe_{80.8}Ti_{7.7}$ alloy (sample 2), the Fe_2Sm phase exists instead of the α-Fe phase. The

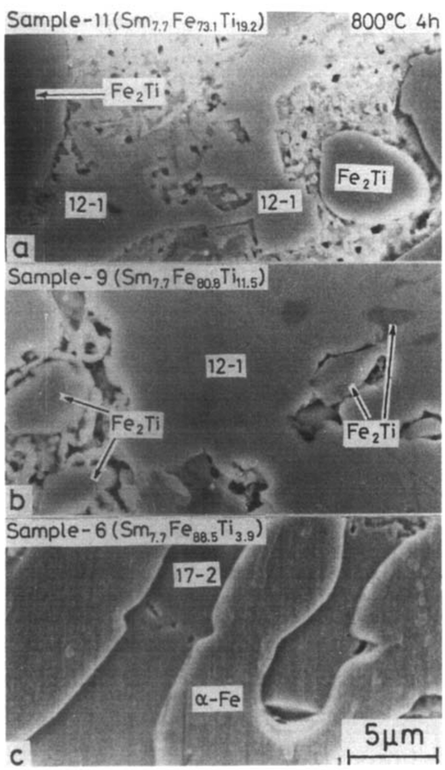

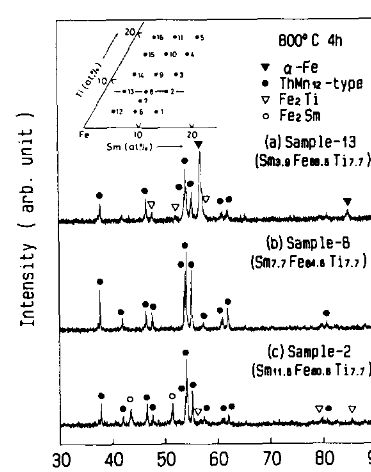

Fig. 3. SEM microstructures taken from (a) $Sm_{7.7}Fe_{73.1}Ti_{19.2}$ (sample 11), (b) $Sm_{7.7}Fe_{80.8}Ti_{11.5}$ (sample 9), and (c) $Sm_{7.7}Fe_{88.5}Ti_{3.9}$ (sample 6) annealed at 800 °C for 4 h.

Fig. 4. X-ray diffraction patterns of (a) $Sm_{3.9}Fe_{88.5}Ti_{7.7}$ (sample 13), (b) $Sm_{7.7}Fe_{84.6}Ti_{7.7}$ (sample 8), and (c) $Sm_{11.5}Fe_{80.8}Ti_{7.7}$ (sample 2) annealed at 800 °C for 4 h.

microstructures of the samples in Fig. 4 are shown in Fig. 5. The matrix phase is identified as $SmFe_{11}Ti$ and the Fe_2Ti phase exists around the α-Fe(Ti) in the $Sm_{3.8}Fe_{88.5}Ti_{7.7}$ alloy (sample 13) (Fig. 5(a)). The $Sm_{7.7}Fe_{84.6}Ti_{7.7}$ alloy (sample 8) is nearly single phase and consists of $SmFe_{11}Ti$. Small amounts of the Fe_2Ti phase exist along the grain boundary (Fig. 5(b)). The Fe_2Sm phase can be observed in the $Sm_{11.5}Fe_{80.8}Ti_{7.7}$ alloy (sample 2) (Fig. 5(c)).

Figure 6 shows the isothermal section of the Sm–Fe–Ti system at 800 °C. The Fe_7Sm phase mentioned by Jang *et al.* [9], could not be observed in our study, but the existence of five compounds around the $SmFe_{11}Ti$ (12–1) compound can be confirmed. The phase regions which appeared in the Sm–Fe–Ti system are characterized by two-phase and three-phase fields between the compounds $SmFe_{11}Ti$ (12–1), Fe_2Ti, α-Fe(Ti), $Fe_{17}Sm_2$ (17–2), Fe_3Sm (3–1) and Fe_2Sm (2–1). When the titanium content increases from that of $SmFe_{11}Ti$ (12–1) compound, the Fe_2Ti and Fe_2Sm (2–1) phases will appear. So, three phases including the $SmFe_{11}Ti$ (12–1) compound coexist in this region. The $Sm_{7.7}Fe_{76.9}Ti_{15.4}$ alloy (sample 10), which corresponds to $SmFe_{10}Ti_2$, is included in this region. When the samarium concentration decreases from that of $SmFe_{11}Ti$ (12–1), however, the α-Fe(Ti) and Fe_2Ti phases will appear at the expense of the $SmFe_{11}Ti$ (12–1) compound. When the titanium concentration decreases from that of $SmFe_{11}Ti$ (12–1), α-Fe(Ti) and $Fe_{17}Sm_2$ (17–2) are formed coexisting with the $SmFe_{11}Ti$ (12–1) compound.

3.2. Isothermal section of the Sm–Fe–Ti system for the iron-rich corner at 1000 °C

The phases of ingots annealed at 1000 °C and in the as-cast state were also studied by X-ray diffractions, optical microscopy and SEM–EDX. It

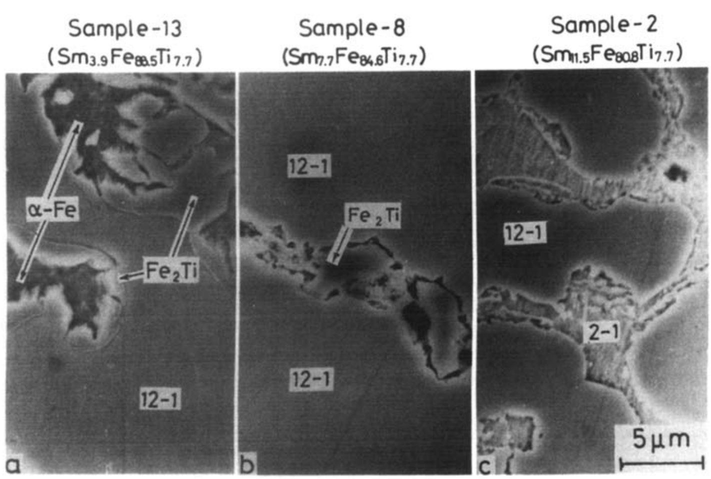

Fig. 5. SEM microstructures taken from (a) $Sm_{3.9}Fe_{88.5}Ti_{7.7}$ (sample 13), (b) $Sm_{7.7}Fe_{84.6}Ti_{7.7}$ (sample 8), and (c) $Sm_{11.5}Fe_{80.8}Ti_{7.7}$ (sample 2) annealed at 800 °C for 4 h.

turned out that the resultant phases in the cast ingots were almost the same as those found in samples annealed at 800 °C on the samarium-poor side. However, on the samarium-rich side, the phase relations were different from those at 800 °C. Figure 7 shows the microstructure of an $Sm_{11.5}Fe_{84.6}Ti_{3.9}$ alloy (sample 1) annealed at 1000 °C for 4 h. It was found from SEM–EDX analysis that this alloy consisted of $Fe_{17}Sm_2$ (17–2) and a samarium-rich phase. This samarium-rich phase is liquid at 1000 °C judging from the samarium content of this phase.

Furthermore, it was found that another high temperature phase appeared in samples annealed at 1000 °C. Figure 8 shows the X-ray diffraction patterns of the $Sm_{11.5}Fe_{69.2}Ti_{19.2}$ alloy (sample 5) annealed at (a) 1000 °C and (b) 800 °C. The diffraction peaks of an unknown phase can be observed in the alloy annealed at 1000 °C. This unknown phase accompanied additional diffraction lines with strong intensity at $d=2.295$ Å which is very close to that of the metastable κ phase reported in ref. 12. Figure 9 shows the optical microstructure of the $Sm_{11.5}Fe_{69.3}Ti_{19.2}$ alloy (sample 5) annealed at (a) 1000 °C and (b) 800 °C. The square phase, which is indicated by κ, exists in the alloys annealed at 1000 °C and can be considered as the high temperature phase shown in Fig. 8(a). An SEM image taken from the $Sm_{11.5}Fe_{69.3}Ti_{19.3}$ alloy (sample 5) annealed at 1000 °C is shown in Fig. 10. This alloy is composed of three phases: a dark, a grey and a white phase. The SEM–EDX analysis revealed the composition of these three phases. The dark phase is identified as the Fe_2Ti phase. The white phase can be considered as the

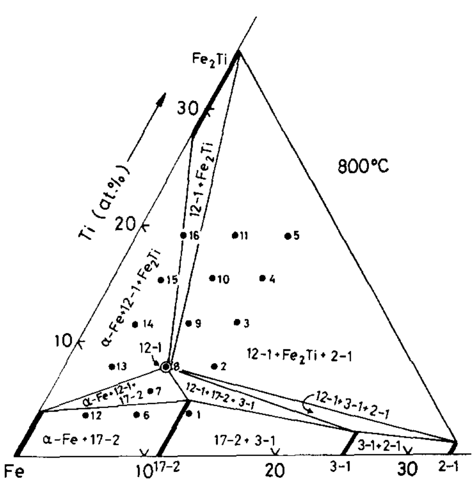

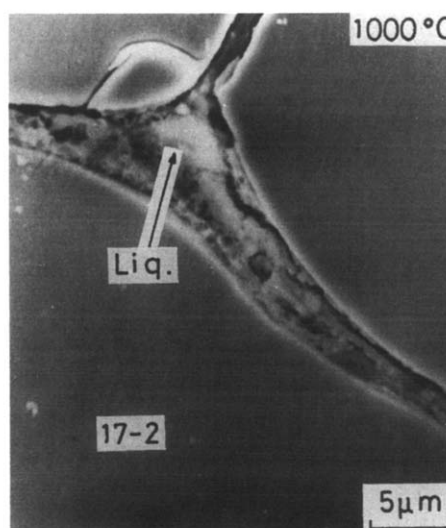

Fig. 6. Isothermal section of the iron-rich corner of the Sm–Fe–Ti ternary phase diagram at 800 °C.

Fig. 7. An SEM microstructure taken from the $Sm_{11.5}Fe_{84.6}Ti_{3.9}$ alloy (sample 1) annealed at 1000 °C for 4 h.

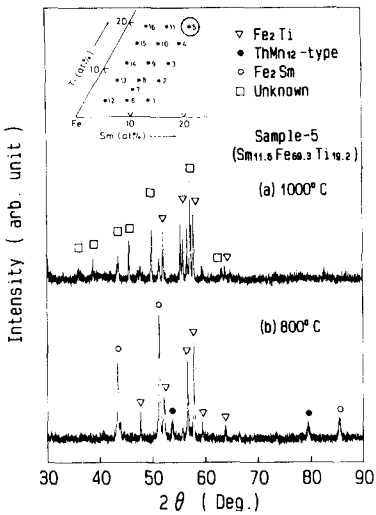

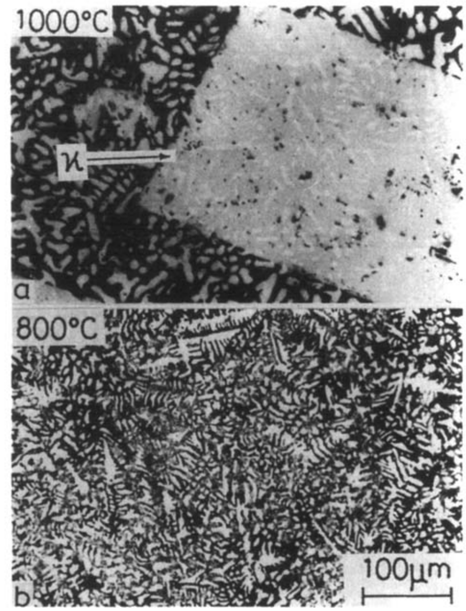

Fig. 8. X-ray diffraction patterns taken from $Sm_{11.5}Fe_{69.3}Ti_{19.2}$ (sample 5) annealed at (a) 1000 °C and (b) 800 °C.

Fig. 9. Optical microstructures taken from $Sm_{11.5}Fe_{69.3}Ti_{19.2}$ (sample 5) annealed at (a) 1000 °C and (b) 800 °C. The κ phase can be considered as a high temperature phase.

liquid phase at 1000 °C judging from the samarium content. The grey phase is the square phase κ shown in Fig. 9(a) which has a samarium-to-iron ratio close to that of $SmFe_{11}Ti$, but is richer in titanium. The composition of the phase is identified as $SmFe_9Ti_2$. This $SmFe_9Ti_2$ phase is the same as that which is called the 11–1 phase by Jang *et al.* [9]. The $SmFe_9Ti_2$ (11–1) phase can be observed in samarium-rich alloys with high titanium contents, *i.e.* $Sm_{11.5}Fe_{88.5-y}Ti_y$ ($7.7<y<19.2$) (samples 2–5) and $Sm_{7.7}Fe_{92.3-y}Ti_y$ ($y=15.4$, 19.2) (samples 10 and 11).

Figure 11 shows the isothermal section at 1000 °C of the Sm–Fe–Ti system in the iron-rich corner. The samarium-poor side of this section is almost the same as that at 800 °C, but in the samarium-rich side, the liquid and $SmFe_9Ti_2$ (11–1) phases appear instead of Fe_3Sm and Fe_2Sm.

3.3. *Magnetic properties of the Sm–Fe–Ti system*

Figure 12 shows the variations of magnetization intensities for Sm_x-$Fe_{100-y}Ti_y$ alloys after annealing at (a) 800 °C and (b) 1000 °C. The magnetization of the Sm–Fe–Ti system increases gradually towards the iron corner of the diagrams. This behaviour is almost independent of the annealing temperature. However, the magnetization of iron-poor samples (upper right portion in Fig. 12) annealed at 1000 °C is much lower than that of samples annealed at 800 °C. Since the $SmFe_9Ti_2$ (11–1) phase exists in the iron-

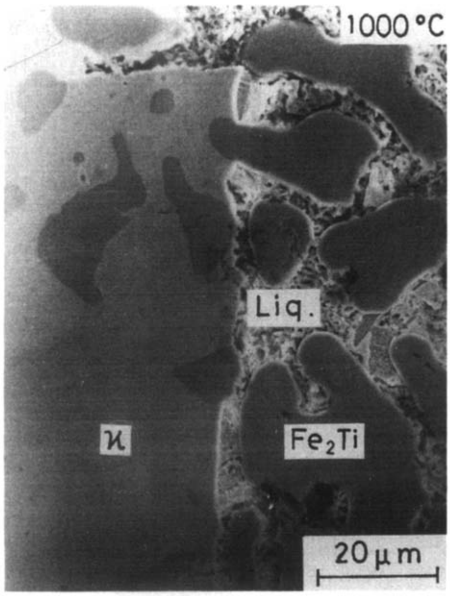

Fig. 10. An SEM microstructure taken from $Sm_{11.5}Fe_{69.3}Ti_{19.2}$ (sample 5) annealed at 1000 °C. The κ phase is identified as $SmFe_9Ti_2$ by SEM–EDX.

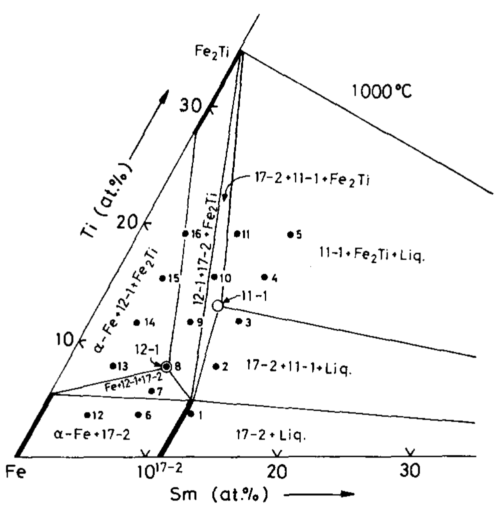

Fig. 11. Isothermal section of the iron-rich corner of the Sm–Fe–Ti ternary phase diagram at 1000 °C.

poor side of the isothermal section at 1000 °C (see Fig. 11), it is apparent that the lower value of magnetization is due to the occurrence of the high temperature phase at the expense of the $SmFe_{11}Ti$ (12–1) compound. This result also suggests that the $SmFe_9Ti_2$ (11–1) phase is non-magnetic or weakly magnetic. Since the ingots studied show coercive force below 1 kOe,

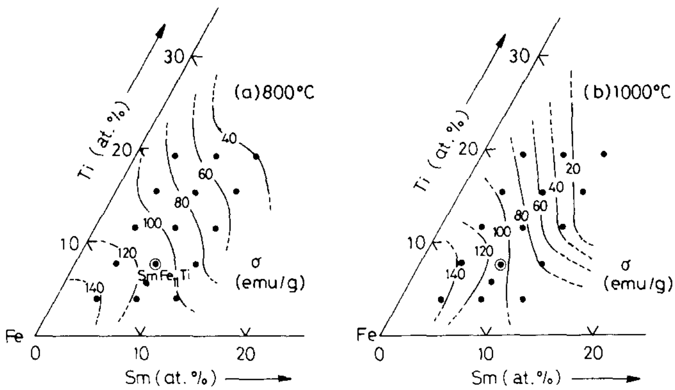

Fig. 12. The magnetization of samples annealed at (a) 800 °C and (b) 1000 °C.

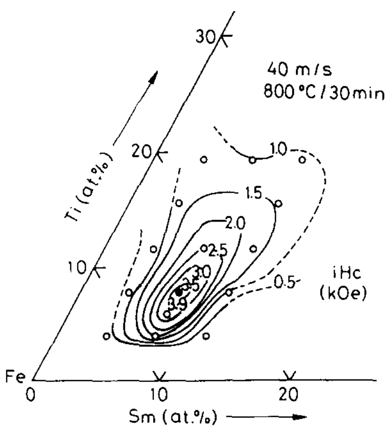

Fig. 13. The isocoercivity lines of Sm–Fe–Ti melt-spun samples. The alloys were overquenched with a surface velocity of 40 m s^{-1} and then annealed at 800 °C for 30 min in a samarium atmosphere.

melt-spinning was adopted to optimize the composition of high coercivity.

Figure 13 shows the coercivity of melt-spun Sm–Fe–Ti ribbons as a function of composition. The ribbons were overquenched with a surface velocity of 40 m s^{-1} followed by annealing at 800 °C for 30 min. The highest coercivity of 3.9 kOe among the studied alloys was obtained for the $SmFe_{11}Ti$ (12–1) compound. Since the isocoercivity lines have such an elongated shape, the samarium content will be the component most sensitive to coercivity. In fact, the severe loss of samarium during annealing, especially of melt-spun ribbons, caused the decrement of coercive force, or step demagnetization curves [5, 6, 10, 11]. Therefore, annealing in the samarium atmosphere [6, 10] is strongly recommended to obtain high coercivity in samarium-containing melt-spun $ThMn_{12}$-type magnets.

Acknowledgment

The authors would like to thank Mr. Akihiko Kojima for his helpful discussions.

References

1 D. B. de Mooij and K. H. J. Buschow, *J. Less-Common Met.*, *136* (1988) 207.
2 K. H. J. Buschow, *J. Appl. Phys.*, *63* (1988) 3130.
3 K. Ohashi, T. Yokoyama, R. Osugi and Y. Tawara, *IEEE Trans. Magn.*, *23* (1987) 3101.
4 J. Ding and M. Rosenberg, *J. Magn. Magn. Mater.*, *80* (1989) 105.
5 J. Strzeszewski, Y. Z. Wang, E. W. Singleton and G. C. Hadjipanayis, *IEEE Trans. Magn.*, *25* (1989) 3309.
6 M. Okada, A. Kojima, K. Yamagishi and M. Homma, *IEEE Trans. Magn.*, *26* (1990) 1376.
7 L. Schultz, K. Schnitzke and J. Wecker, *Appl. Phys. Lett.*, *56* (1990) 868.
8 K. Ohashi, Y. Tawara, R. Osugi and M. Shimao, *J. Appl. Phys.*, *64* (1988) 5714.
9 T. S. Jang and H. H. Stadelmaier, *J. Appl. Phys.*, *67* (1990) 4957.
10 K. Yamagishi, M. Okada and M. Homma, in K. J. Strnat and T. Shinjo (eds.), *Proc. 10th Int. Workshop on Rare-Earth Magnets and Their Applications*, Vol. 1, The Society of Non-Traditional Technology, Tokyo, 1989, p. 217.
11 K. Ohashi, Y. Tawara and R. Osugi, *J. Less-Common Met.*, *139* (1988) L1.
12 K. Schnitzke, L. Schultz, J. Wecker and M. Katter, *Appl. Phys. Lett.*, *56* (1990) 587.